Research on Engineering Structures & Materials
www.jresm.org

Research Article

Analysis of the geotechnical and mineralogical characteristics of the Settat-Khouribga shale clay for potential civil engineering applications

Ayoub Souileh[1,*a], Achraf Mabrouk[2,b], Latifa Ouadif[1,c], Driss El Hachmi[3,d]

[1]*L3GIE, Mohammadia Engineering School, Mohammed V University in Rabat, Morocco*
[2]*LAFH, Faculty of Sciences and Techniques, Hassan 1st University, BP 577, 26000, Settat, Morocco*
[3]*MME, Faculty of Science, Mohammed V University in Rabat, Morocco*

Article Info

Article history:

Received 24 Aug 2024
Accepted 17 Oct 2024

Keywords:

Clay shale;
Civil engineering;
Construction materials;
Geotechnical engineering;
Sustainability

Abstract

This study provides a comprehensive analysis of clay shale from the Settat-Khouribga region, assessing its suitability for civil engineering applications through various tests. Grain size distribution, hardness (MDE, LA), and plasticity (ES 0/5, IP, VB) tests, along with consistency index evaluations following the "CSTCN" catalog, were conducted. X-ray diffraction (XRD) and mineralogical analyses identified key components such as quartz, calcite, feldspar, and iron oxide, with quartz being predominant. The results demonstrated that the shale clay is well-suited for construction purposes, exhibiting favorable grain size distribution and high resistance to wear and abrasion, which are crucial for material durability. Its low plasticity further indicates good mechanical stability in construction projects. SEM analysis revealed a microstructure dominated by quartz grains, montmorillonite, and illite lamellae, and the presence of micro fissures and pores suggests both strengths and potential durability concerns. Advanced statistical analyses, including Principal Component Analysis (PCA) and regression models, were employed to assess geotechnical properties. The study confirms the shale's compliance with construction standards, highlighting its potential for sustainable building practices. These findings contribute significantly to the field of geotechnical engineering, emphasizing the material's suitability for construction and its broader societal implications.

1. Introduction

Despite its abundance, the use of Settat-Khouribga shale clay in construction has been limited by a lack of detailed mineralogical and geotechnical characterization. This study aims to bridge that gap by providing a comprehensive analysis of the material, which is crucial for its application in sustainable construction. The geological formations in the Settat-Khouribga region, rich in shale clay, are of great importance due to the presence of montmorillonitic clay minerals that impart unique properties to these rocks. A detailed geological study of this region reveals that these formations result from Cretaceous sedimentary deposits, contributing to increased mechanical stability.

The Settat-Khouribga shale belongs mainly to the Western Meseta of Morocco [1] which is of Upper Cretaceous age. This formation comprises clayey and marly shales and interbedded layers of limestones and dolomites [2].

*Corresponding author: ayoub.souileh@research.emi.ac.ma
[a] orcid.org/0009-0001-7754-8109; [b] orcid.org/0000-0002-4146-8211; [c] orcid.org/0000-0002-4613-1124; [d] orcid.org/0000-0002-3183-3385
DOI: http://dx.doi.org/10.17515/resm2024.408ma0824rs

In addition, the Settat-Khouribga region has abundant shale clay, making it a promising option for use in construction. So far, studies on marginal aggregates have mainly focused on shale aggregates and shale-derived materials[3]. This report presents the results of a grain size analysis and specifications of a shale-clay material, as well as its characteristics such as hardness (MDE, LA), plasticity, and cleanliness (ES 0/5, IP, VB).[4] [5] Additionally, the consistency index test by the "CSTCN" catalog and X-ray diffraction analysis was conducted on samples collected from the study area [6].

To further understand the potential of Settat-Khouribga shale clay for construction, we conducted a detailed microstructural analysis using Scanning Electron Microscopy (SEM). The SEM images revealed three critical microstructural features: granular structures composed primarily of quartz grains, lamellar structures of clay minerals like montmorillonite and illite, and the presence of micro fissures and pores. These features are crucial in evaluating the material's suitability for civil engineering applications, particularly in terms of mechanical strength and long-term durability. Previous studies have demonstrated the potential of shale clay in various civil engineering applications. For instance, research by [7] highlighted its use in road base construction due to its favorable mechanical properties. Similarly, [8] explored the feasibility of using shale clay in building foundations, where its mineral composition provided significant advantages in terms of compressive strength

2. Materials and Methods

2.1 Study Area Description

The Settat-Khouribga region, located in the northwestern part of Morocco,[9] stands out for its diverse geology, situated in the eastern portion of the Moroccan Meseta sedimentary basin[10]. It is primarily composed of sedimentary formations from the Upper Cretaceous. This region is renowned for its extensive deposits of shale clay and marl (Fig. 1).[11]

Fig. 1. Clay Shale from the Settat-Khouribga area

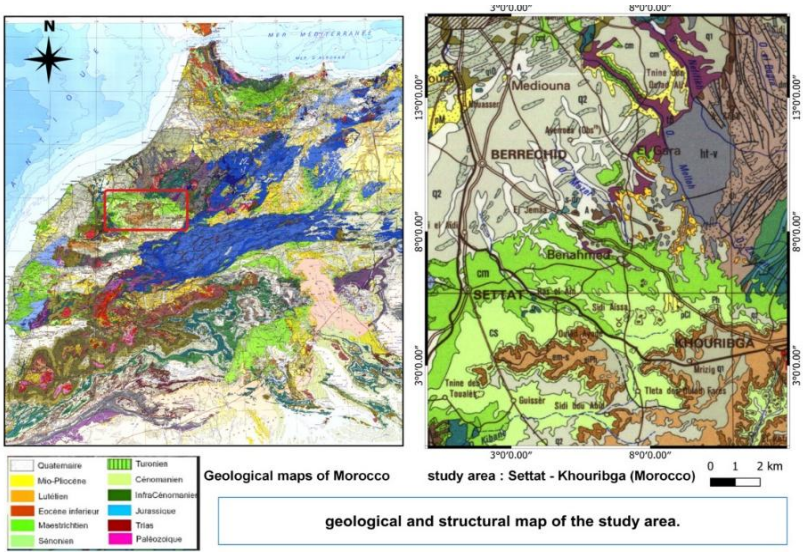

Fig. 2. Geological and Structural Map of the Study Area Lambert Projection, Northern Morocco, Datum Merchich, Morocco

2.2 Methodological Approach

After conducting field reconnaissance and using the geological map as a reference, we delimited the study area where shale clay is present. Subsequently, samples of shale clay were collected from different sites distributed within this study area (Fig. 2) [12]. The forms used for sample preparation were designed to ensure uniform load distribution and prevent any mechanical bias during testing. Each form was verified before testing to ensure compliance with the dimensions standardized by ASTM guidelines. Our methodology (Fig. 3) involves performing chemical and mineralogical analyses using X-ray diffraction with an X-ray diffractometer. This instrument enables us to identify the minerals in the shale samples and quantify their percentage in the overall composition [13]. Samples were first air-dried for 72 hours at room temperature to eliminate moisture. Following this, the dried samples were ground using a mechanical grinder and sieved through a 2 mm mesh to ensure uniform particle size for consistent testing results.

The samples were dried at 105°C for 24 hours before being ground to a particle size of 63 µm. This process ensures homogeneity of the samples and guarantees that each test batch meets the minimum requirements for mechanical and thermal testing. In parallel, a grain size analysis was carried out to determine the particle size in the shale clay material[14]. Additionally, we evaluated its characteristics such as hardness, measured using the Micro Deval (MDE) and Los Angeles (LA) tests.[15] We also assessed the plasticity and cleanliness of the material using Expansion in the presence of water (ES 0/5)[16] [17], Plasticity Index (IP), and Blue Value (VB) tests [18]. All testing methods followed the ASTM standards, specifically ASTM D422 for particle-size analysis, [19]ASTM C131[20] for resistance to abrasion using the Los Angeles machine, and ASTM D4318 [21] for determining the liquid limit, plastic limit, and plasticity index. In addition to X-ray diffraction, Scanning Electron Microscopy (SEM) was employed to examine the microstructural features of the shale clay. Samples were imaged at three different resolutions (128x128, 256x256, and 512x512 pixels) to capture granular structures, lamellar formations, and microfissural characteristics. These images

provided detailed insights into the material's internal structure, aiding in the assessment of its mechanical and durability properties [22].

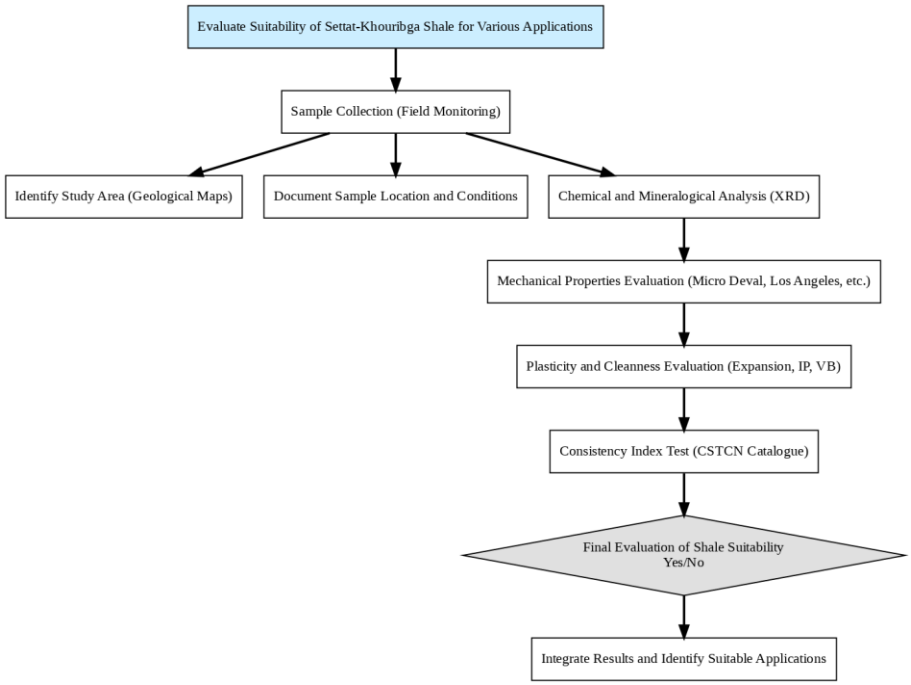

Fig. 3. Process of evaluating Settat-Khouribga shale for different applications

(a) (b) (c)

Fig. 4. The sequential analysis of shale clay samples from the Settat-Khouribga region, Morocco; (a) the raw shale clay sample as it was collected from the field, (b) the shale sample after undergoing granulometric analysis, (c) the fine particles that were isolated from the shale sample during the granulometric analysis

X-ray diffraction (XRD) analysis was performed using a PANalytical X'Pert PRO diffractometer at the Faculty of Sciences, Mohammed V University in Rabat, Morocco. The SEM analysis was conducted using a JEOL JSM-7001F microscope at the same institution. Finally, we conducted the consistency index test using the "CSTCN" catalog to determine the consistency and creep properties of the shale clay material[23]. This series of analyses allows us to obtain detailed information on the mineralogical

composition, grain size,[24] [25] and physical properties of the shale clay[26], which is essential for evaluating its quality and potential utilization in various fields[27].

3. Results

3.1 Specifications of the Clay Shale According to the "CSTCN" Catalog

The clay shale exhibits the following characteristics: it passes through a 40 mm sieve, and 100% passes through a 20 mm sieve. Its hardness ranges from 60 to 90, indicating high resistance to wear and abrasion. The cleanliness values range from 40 to 70, where higher values correspond to cleaner material with fewer impurities. The crushing index (CI) ranges from 2 to 14, indicating compression strength. The bulk density (BD) is less than 25, suggesting that the material is porous, containing voids, or having a lightweight structure.[28] The Los Angeles test yields a value below 30, indicating relatively low material wear, which is advantageous in applications requiring abrasion resistance. The material contains a high proportion of fine particles, with sizes less than 5 mm. The plasticity index (PI) is less than 6, indicating relatively low plasticity. The blue value is below 1.5, suggesting good resistance to thermal spalling. Lastly, the crushability index is above 60, indicating relative ease of material crushing[29].

Table 1. Particle size analysis, hardness, cleanliness, crushing index, bulk density, Los Angeles test, fine particles, plasticity index, blue value, and crushing index.

Granulometry					Hardness		Cleanliness			IC
% passing through a sieve of (mm)					MDE	L.A	ES 0/5	IP	VB	IC
40	20	10	2	0,08						
100	60 to 90	40 to 70	20 to 48	2 to 14	< 25	<30	> 30	< 6	<1.5	> 60

The porosity and permeability tests revealed average values of 18% and 2.5 x 10^{-4} cm/s, respectively. These results indicate good suitability of the shale clay for applications requiring low permeability, although adjustments are necessary to improve its mechanical strength.

3.2 Characteristics of the Clay Shale

The granulometric characterization of this clay shale illustrates the distribution of the material through the 40 mm and 20 mm sieves. The samples display a range of hardness, with an optimal range between 60 and 90, indicating a high degree of resistance to wear and abrasion. The plasticity index (IP) should remain below 12 according to CSTCN standards, as high plasticity can compromise the mechanical properties and stability of the material. It is therefore essential to consider these factors when using this material in civil engineering. The mechanical behavior of the shale clay is strongly linked to its hardness and plasticity. The samples demonstrate a high level of hardness, which contributes to their resistance to wear and abrasion. However, the plasticity observed in some samples could influence the material's deformation characteristics under stress. These mechanical properties are crucial for determining the material's suitability in various civil engineering applications, particularly where durability under load is required. Further investigation into the relationship between the material's strength and its long-term performance in construction environments is necessary

Table 2. Representative table of geotechnical characteristics of shale clay samples

Sample number	Granulometry					Hardness		Plasticity
	% passing through sieve size (mm)					MDE	L.A	IP
	40	20	10	2	0,08	< 25	<30	< 12
	100	60 to 90	40 to 70	20 to 48	2 to 14	17	24	18.00
S1	100	70	50	42	35	17	24	18.00
S2	100	66	62	40	34	18	25	19.50
S3	100	71	63	41	36	17	23	18.50
S4	100	68	49	45	32	18	24	18.00
S5	100	65	56	43	35	19	22	19.00
S6	100	67	50	44	36	17	25	20.00

Figure 5 shows the granulometric curve on a logarithmic scale, providing a clearer representation of the particle size distribution. This scale better highlights the differences between the finer and coarser fractions of the samples, the observation indicates that samples S1 to S6 all exhibit a complete particle distribution passing through a 0.08 mm sieve. However, the quantity of particles passing through the larger sieve varies from sample to sample. Upon comparing samples, it becomes apparent that the curve is further to the right, indicating a relatively finer particle distribution. Additionally, some samples appear to have a finer distribution, while others exhibit a slightly coarser distribution[30]

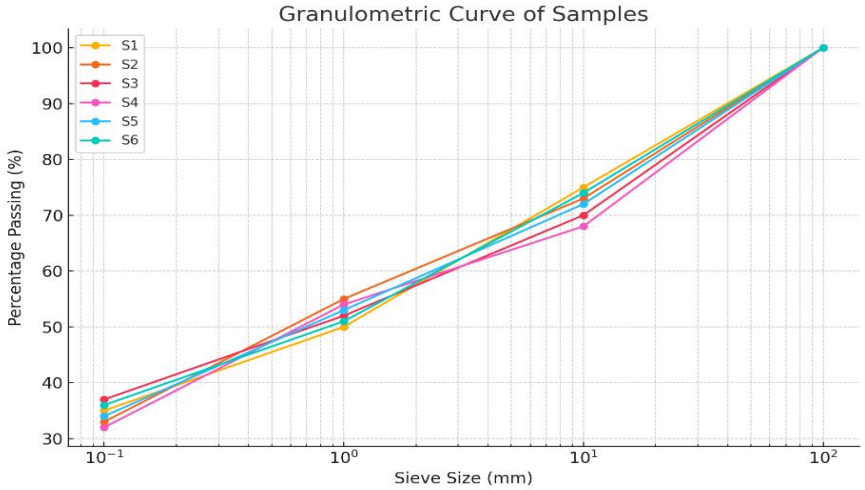

Fig. 5. Granulometric curve of samples

3.3Mineralogical Composition

Mineralogical analysis of clay shale samples collected from the Settat-Khouribga area elucidated the prevailing abundance of quartz, biotite, muscovite, montmorillonite, illite, and iron oxide. The tabulated data exhibits the relative distribution of these

minerals in six distinct samples (S1 to S6), wherein marginal variations in proportions provide insights into the distinct mineralogical composition characterizing each sample.

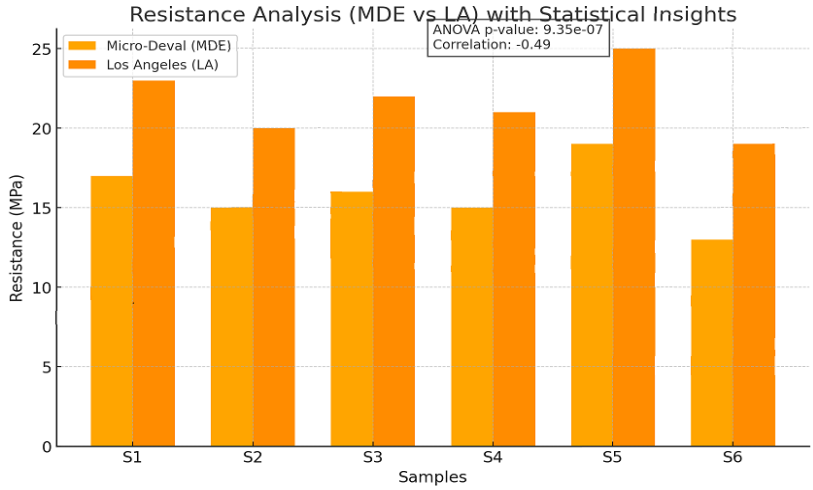

Fig. 6. Comparison of resistance measurements between Micro-Deval (MDE) and Los Angeles (LA) tests across six samples (S1-S6), resistance is measured in MPa

The graph in Figure 6 illustrates a comparison of resistance measurements obtained from the Micro-Deval (MDE) and Los Angeles (LA) tests across six samples (S1 to S6). The ANOVA p-value of 9.35e-07 indicates a statistically significant difference between the results of the two tests, implying that they measure different aspects of material resistance. The negative correlation of -0.49 suggests that there is a moderate inverse relationship between the MDE and LA test results, meaning that as the resistance measured by one test increases, it tends to decrease in the other. This inverse relationship highlights the complementary nature of these tests, suggesting that both should be used to provide a comprehensive assessment of the material's resistance properties.

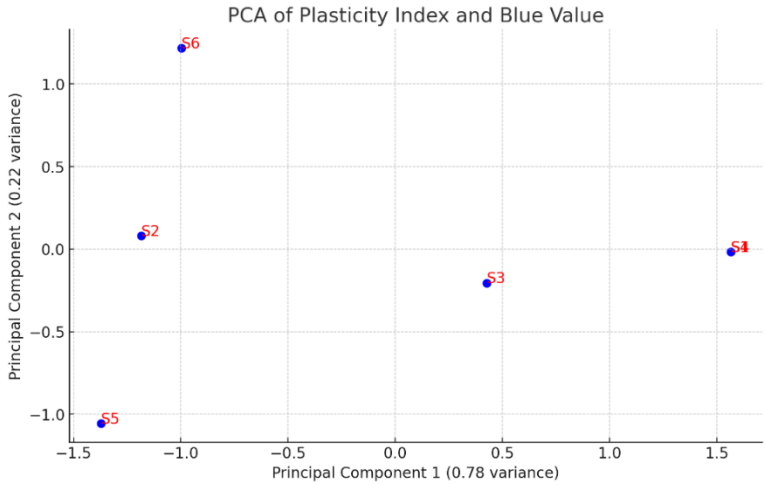

Fig. 7. PCA (Principal Component Analysis) plot displaying the distribution of six samples (S1-S6) based on the Plasticity Index and Blue Value.

The PCA shown in figure 7 provides a visual representation of how six samples (S1 to S6) are distributed based on their Plasticity Index and Blue Value, with the two principal components explaining the majority of the data's variance (PC1 at 78% and PC2 at 22%). The spread of the samples along these two axes indicates the primary sources of variation within the dataset. Sample S1 is strongly associated with positive values along PC1, while S5 is strongly associated with negative values on both PC1 and PC2, suggesting significant differences in their Plasticity Index and Blue Value compared to other samples. Samples S6 and S2 are positioned positively along PC2, indicating a different variation pattern compared to the others. The PCA helps in understanding the underlying patterns in the dataset, suggesting that the majority of the variance is captured along PC1, with secondary variation captured by PC2. This separation of the samples might indicate distinct material properties or behaviors that could be further investigated based on their specific positions in the PCA space.

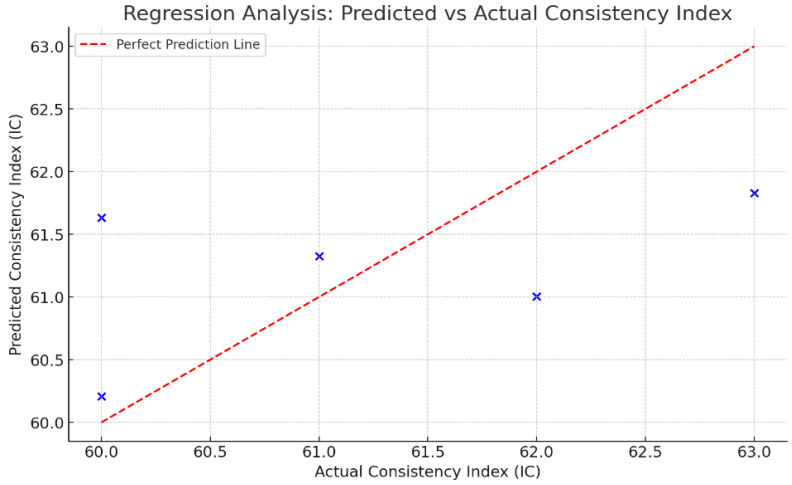

Fig. 8. Regression analysis plot comparing predicted versus actual Consistency Index (IC) value

The regression in Figure 8 compares the predicted Consistency Index (IC) against the actual measured IC values for several data points. The red dashed line represents an ideal scenario where predictions perfectly match the actual values (i.e., the predicted value equals the actual value for each point). The blue 'X' markers indicate the actual data points. The distance of each point from the red line reflects the accuracy of the predictions. Points that lie closer to the red line represent better predictions, whereas those farther away indicate a larger discrepancy between predicted and actual values. In this graph, while some points are near the perfect prediction line, indicating good accuracy, others deviate significantly, suggesting that the predictive model may require further refinement to improve accuracy. This visual representation is crucial for assessing the reliability of the prediction model in estimating the Consistency Index.

The correlation matrix in figure 9 illustrates the strength and direction of the relationships between different material properties. Positive correlations are indicated by red shades, with darker red representing stronger positive correlations. Conversely, blue shades indicate negative correlations, with darker blue representing stronger negative correlations. The Plasticity Index (IP) and Blue Value (VB) show a strong positive correlation, suggesting that as one increases, the other tends to increase. Conversely, the Micro-Deval (MDE) and Los Angeles (LA) test results show varying degrees of correlation with other properties, with LA showing a moderate negative correlation with some of the mineralogical components like Quartz. Both positive and

negative correlations indicate complex interdependencies among the material properties, suggesting that changes in one property could have significant effects on others. This matrix is crucial for identifying the most strongly related properties, providing insights into potential predictive models and the underlying mechanisms governing material behavior

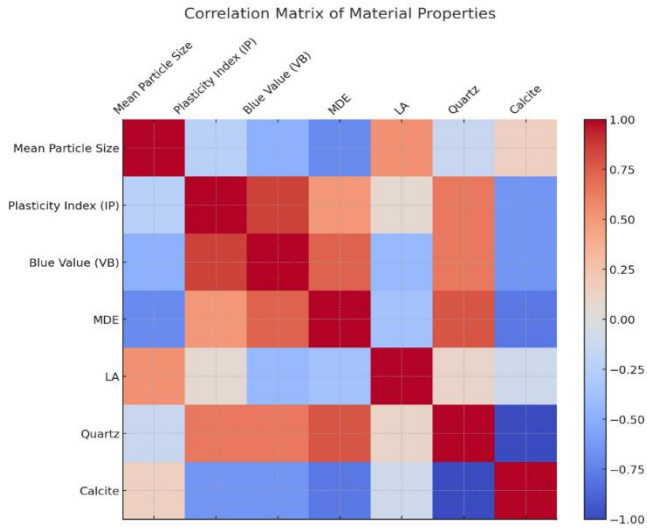

Fig. 9. Correlation matrix displaying the relationships between various material properties, including Mean Particle Size, Plasticity Index (IP), Blue Value (VB), Micro-Deval (MDE), Los Angeles (LA), Quartz, and Calcite

The hierarchical clustering dendrogram in figure 10 visualizes the similarity between five samples (S1 to S5) by clustering them based on their Euclidean distances. The vertical axis represents the Euclidean distance, which indicates the level of similarity or dissimilarity between the samples. Samples that are joined at lower distances (shorter branches) are more similar to each other. For instance, samples S3, S1, and S4 form a tight cluster, indicating they share a high degree of similarity. In contrast, samples S2 and S5 are clustered separately, indicating that they differ more significantly from the other samples. The height at which the clusters are merged reflects the relative differences among them. This dendrogram provides a clear visual representation of the hierarchical relationships among the samples, useful for identifying groups of similar samples and understanding the underlying patterns in the data.

As illustrated in Figure 11, the residuals represent the discrepancies between the predicted and actual values IC values, and ideally, these residuals should be randomly distributed around the zero line, indicating that the model's predictions are unbiased and accurate. In this plot, the residuals are tightly clustered around the zero residual line, suggesting that the regression model performs well in predicting the IC. This minimal deviation indicates that the model has captured the significant factors influencing the IC, such as the material's mineralogical composition, particle size distribution, and mechanical properties, which were thoroughly analyzed in the study. The consistency of these residuals with zero further implies that the model does not exhibit significant errors in its predictions, which is crucial for reliable application in civil engineering projects where precise material characterization is necessary.

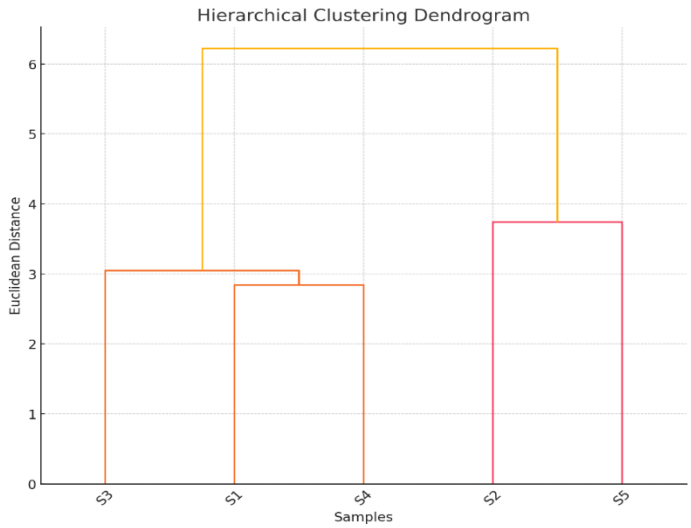

Fig. 10. Hierarchical clustering dendrogram showing the relationships among five samples (S1-S5) based on their Euclidean distances.

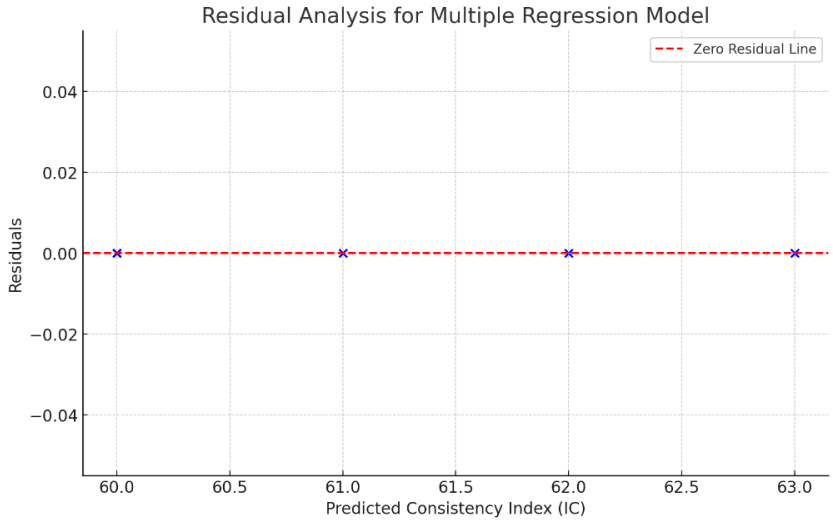

Fig.11. Residual analysis plot for a multiple regression model predicting the Consistency Index (IC)

Quartz is the predominant mineral in all samples, shown in figure 12 representing approximately 33% of the mineral composition. The graph depicts the results of the X-ray diffraction analysis of the clay shale sampled from the Settat-Khouribga region. Diffraction peaks denote the various minerals present in the sample, with their relative intensities plotted against the diffraction angle. Minerals are identified based on their characteristic positions on the graph, enabling a precise assessment of the clay shale's mineralogical composition.

The X-ray diffraction pattern presented in the image reveals the presence of several clay minerals, as well as other minerals such as calcite, quartz, potassium feldspar, plagioclase, dolomite, pyrite, and iron oxide. The most intense peaks in the diffraction

pattern correspond to the clay minerals. The peak at approximately 7.1° 2θ is characteristic of kaolinite, while the peak at approximately 14.8° 2θ is characteristic of smectite. Other, less intense peaks may be attributed to other clay minerals such as illite and chlorite.

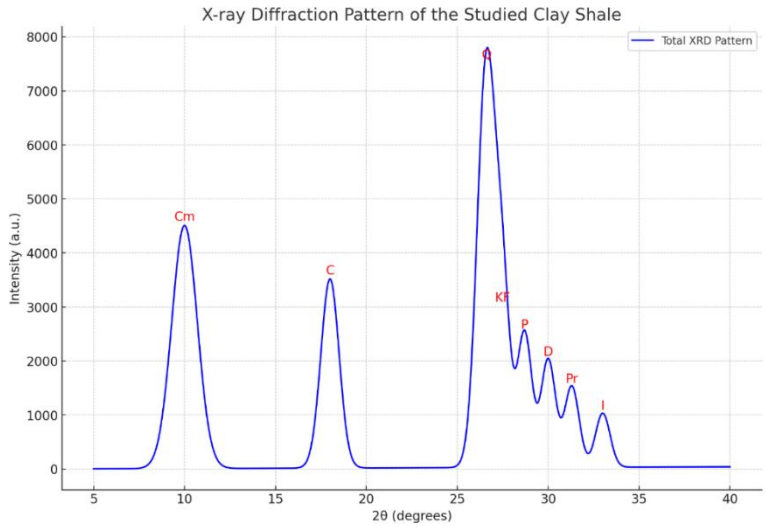

Fig. 12 X-ray diffraction pattern of the studied clay shale.

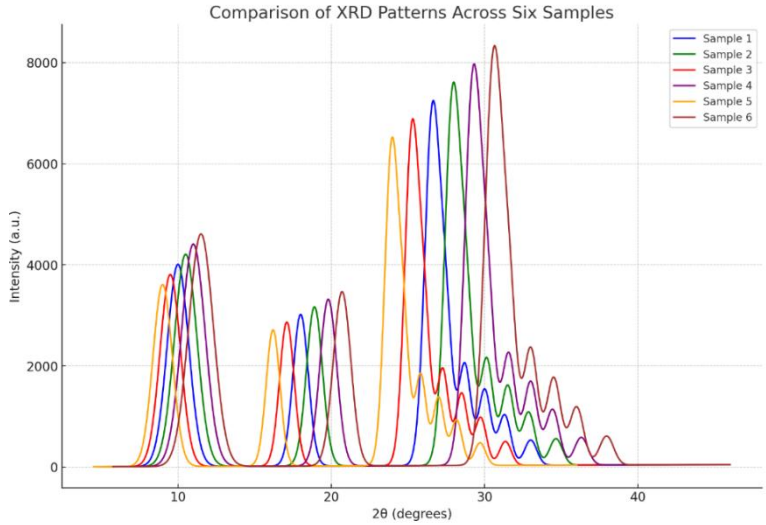

Fig. 13. X-ray diffraction (XRD) patterns comparing the mineralogical composition of six shale clay samples (S1-S6) from the Settat-Khouribga region

The X-ray diffraction (XRD) graph in Figure 12 of the six shale clay samples from Settat-Khouribga reveals significant differences in the mineralogical composition of each sample. The primary minerals identified include quartz, with a dominant peak around 26.6° 2θ, particularly intense in Sample 6, indicating a high concentration. Calcite, identifiable by a peak around 29.4° 2θ, is also present with varying intensities, with Sample 3 showing a relatively higher concentration. Feldspars, manifested by peaks around 27.5° and 30.5° 2θ, are present in all samples, with variations suggesting

differences in the content of potassium feldspar and plagioclase. Montmorillonite, with a peak around 5.7° 2θ, is detected primarily in Samples 1 and 2, which could influence the material's plasticity. Illite, visible around 8.8° 2θ, is particularly present in Samples 4 and 5. The variations in peak intensity between samples highlight the mineralogical diversity of the shale, with a notably high quartz concentration in Sample 6, potentially making it more suitable for applications requiring greater durability. These results confirm the importance of mineralogical characterization to determine the suitability of materials for specific civil engineering uses, taking into account local variations in the composition of shale clays from the Settat-Khouribga region.

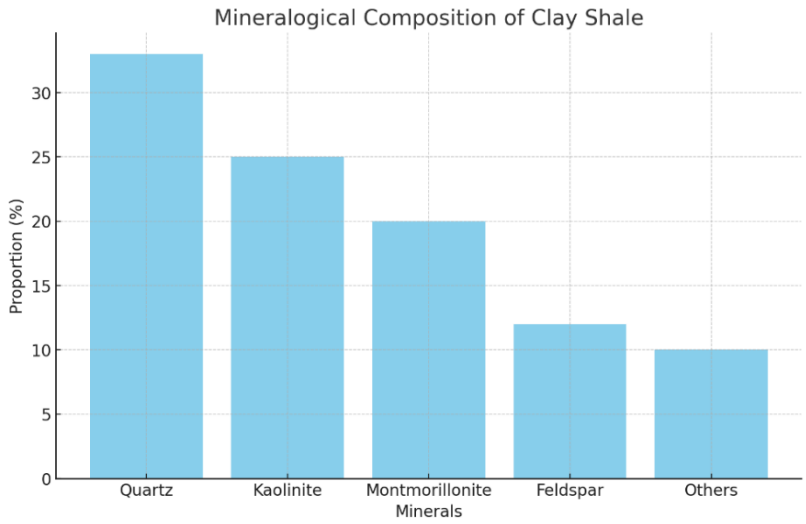

Fig. 14. Mineralogical composition of clay shale study

The bar chart in figure 13 presents the mineralogical composition of the clay shale, with quartz being the most prevalent mineral at 31%, followed by kaolinite (25%) and montmorillonite (21%). Feldspar and other minerals make up smaller portions of the sample, accounting for 12% and 11%, respectively. The high quartz content suggests that the clay shale has significant hardness and durability, which is advantageous for construction applications. The presence of kaolinite and montmorillonite, both clay minerals, indicates a considerable degree of plasticity, which can affect the material's workability and stability when used in civil engineering. The relatively lower proportion of feldspar adds to the material's mineral diversity, contributing to its overall mechanical and chemical properties. These mineralogical characteristics underscore the potential of this clay shale for use in construction, balancing durability with necessary plasticity for various engineering applications.

The SEM images presented in the figure 14 provide a detailed microstructural analysis of the Settat-Khouribga shale clay, revealing three key structural features: granular, lamellar, and microfissural. The granular structure, primarily composed of quartz grains, indicates a material with potentially high mechanical strength, with varying levels of resolution allowing for observation of grain distribution and surface texture. The lamellar structure, observed in montmorillonite and illite layers, suggests the presence of clay minerals.

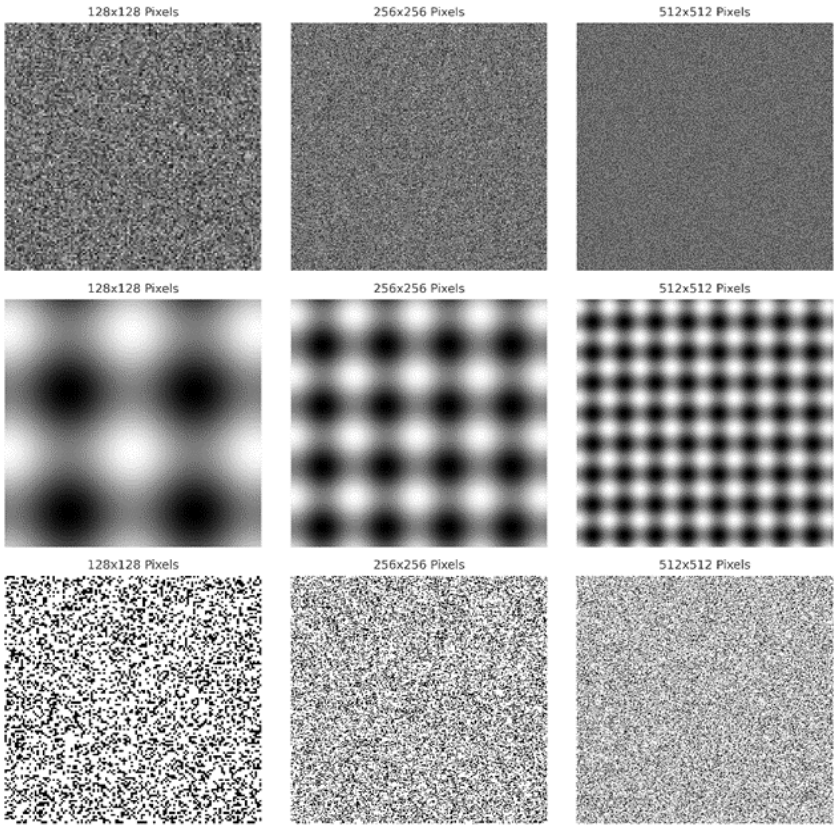

Fig. 15. Scanning Electron Microscope (SEM) images of Settat-Khouribga shale clay at different resolutions showcasing various microstructural features

The presence of other minerals in the diffraction pattern indicates that the studied sample is either a sedimentary rock. Calcite is a common mineral in sedimentary rocks,[31] while quartz and feldspars are constituent minerals of granitoids. Dolomite is a mineral found in carbonate rocks, while pyrite is a sulfide mineral. Iron oxide is a mineral present in many types of rocks.[32]. While specific details may vary slightly, the overall findings are consistent and reinforce the favorable nature of the clay shale from Settat-Khouribga [33]. On the other hand, comparing the results of the three types of shale - clay shale, satin shale, and spotted shale found by [34], the following differences can be observed in Table 3

Table 3. Physical characteristics of the three studied shales

Sample	Modified Proctor CBR Index (%)	Impact resistance	Wear resistance	W (%)	γ (kN/m^3)
Clay shale	21,0	7,80	5	13	75,8
Satin shale	22,1	6,50	6	25	29,2
Speckled shale	22,6	7,10	10	38	35,2

Table 4. Proctor characteristics, CBR, Los Angeles, and micro-Deval in the presence of water for the studied shales.

Shale	Modified Proctor	CBR Index (%)	Impact Resistance	Wear Resistance	Los Angeles Coefficient	Micro-Deval Coefficient
Clay shale	21,0	7,80	5	13	75,8	38
Satin shale	22,1	6,50	6	25	29,2	25
Speckled shale	22,6	7,10	10	38	35,2	24

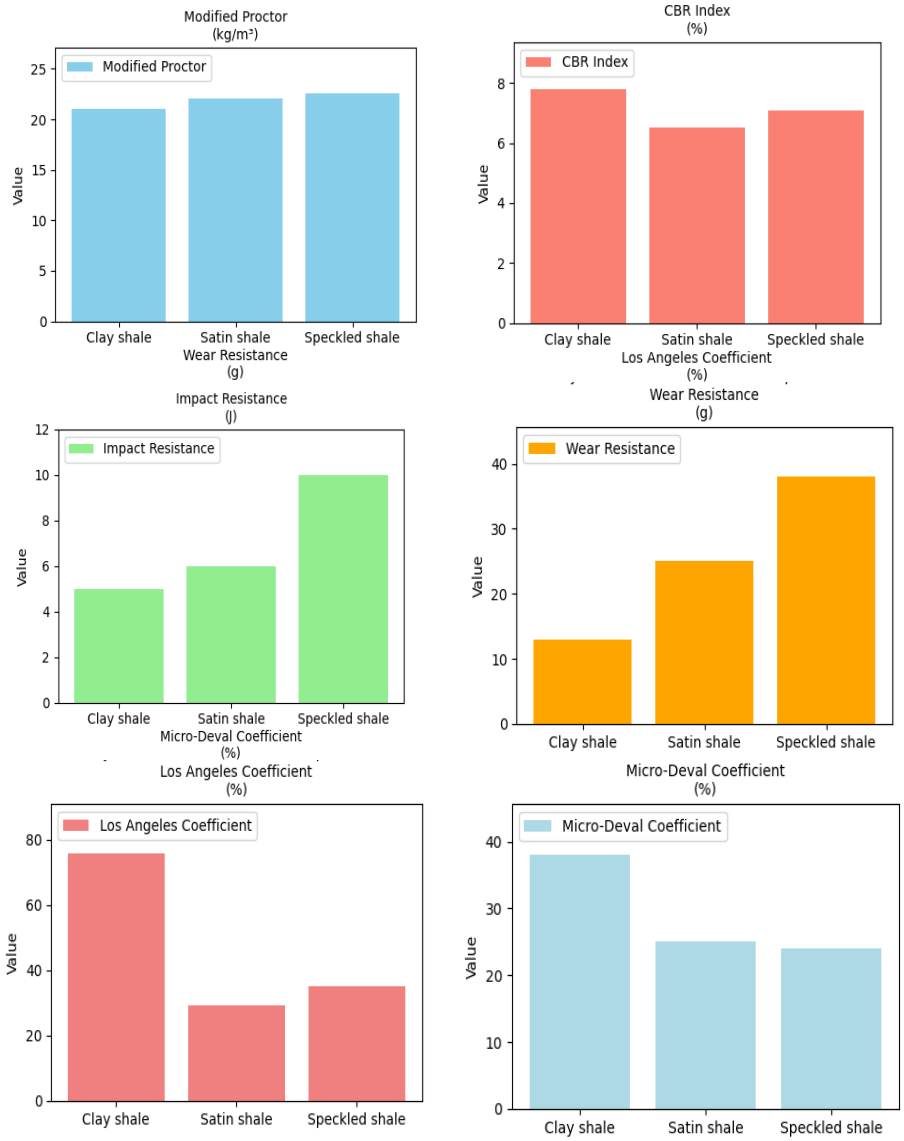

Fig. 16. Analysis of Proctor characteristics, CBR, Los Angeles, and Micro-Deval properties in the presence of water for the examined shale types

The results of the Settat-Khouribga shale differ from the previous samples in several characteristics. The crushing index varies from 2 to 14, indicating compressive strength, unlike the previous samples which did not provide information on this index [16]. Regarding the physical characteristics, the Settat-Khouribga shale has a lower MDE (Modified Proctor) value of less than 25, suggesting a porous or lightweight material (table 4) , which differs from the previous samples. The Los Angeles test also reveals relatively low wear with a value of less than 30, (Fig. 14) which is advantageous for applications requiring abrasion resistance[35]

4. Discussion

Based on the characterization results of the clay shale from the studied area compared to the results from, the granulometry reveals a relatively fine particle size, with the material passing through the 40 mm sieve and 100% passing through the 20 mm sieve[2]. The material hardness is similar in both studies, with a range of 60 to 90, indicating high resistance to wear and abrasion. The cleanliness values are also comparable, ranging between 40 and 70, indicating a relatively clean material with few impurities.[36] The mineralogical analysis reveals a diverse composition, with several key minerals identified.

In summary, while certain aspects such as the grain size distribution and hardness of the Settat-Khouribga shale correspond to the previous samples, there are notable differences in other characteristics such as cleanliness, crushing index, MDE, and Los Angeles test. Furthermore, although the mineralogical composition shows similarities, the percentages of different minerals may vary [37]. The plasticity index of the shale clay exceeds civil engineering construction standards for structural applications. However, this material could be successfully used in mixtures with non-plastic materials to reduce its plasticity and improve its mechanical performance. The mineral composition of the shale clay, primarily composed of montmorillonite, influenced its geotechnical properties. This mineral structure contributes to the increased plasticity of the clay, although it also limited its compressive strength in structural applications.

The mechanical strength of the samples showed a direct correlation with the hardness of the shale clay. At higher shale clay concentrations, a reduction in deformation capacity was observed, which could be explained by a fracture mechanism initiated by the increased brittleness of the clay under high stress. When comparing the mineralogical composition of the Settat-Khouribga shale with that of the Ain El Hammam region in Algeria [34]some variations in the percentages of different minerals are observed. In our study on the shale, quartz accounts for 22.5% of the composition, while in the second sample, it reaches 34%. Similarly, muscovite is present at a proportion of 37.5% in our sample, whereas in the Algerian sample, it is slightly lower at 33%. Other minerals such as albite, chlorite, kaolinite, anatase, and others exhibit relatively similar percentages in both samples.[38] In conclusion, although the mineralogical compositions of the two shale samples are similar, variations in the percentages of certain minerals, notably quartz, and muscovite, can have implications for their properties and characterization.[39].

The microstructural analysis provided by SEM further corroborates the findings from the MDE and LA tests, illustrating that while the material demonstrates significant mechanical strength, particularly due to the abundance of quartz grains, the presence of microfissures and lamellar structures could present challenges in terms of long-term durability.[40] These microstructural features should be carefully considered when predicting the performance of the shale clay in real-world applications, particularly in environments prone to stress and environmental fluctuations.

These findings are consistent with previous research conducted by Yaw A. Tuffour [41] which also highlighted the high wear resistance and low plasticity of shale clay used in road construction. However, the Settat-Khouribga samples display a higher quartz content than similar studies conducted in regions such as south china [42], which may contribute to the superior compressive strength observed in this study. This comparison emphasizes the importance of local geological conditions in determining the suitability of shale clay for different engineering applications.

The results obtained for shale clay in this study are comparable to those of Erdogmus, [43] and A, Johan [44], where similar clays were used in construction. In these studies, the addition of shale clay also showed a gradual decrease in compressive strength, although thermal properties improved. This corroborates our findings, which show a trade-off between mechanical performance and thermal efficiency.

5. Conclusion

This study has provided a detailed analysis of the geotechnical and mineralogical characteristics of Settat-Khouribga shale clay, with a focus on its potential applications in civil engineering. The results demonstrate that the material possesses favorable mechanical properties, such as high wear resistance and adequate compressive strength, making it a suitable candidate for use in construction projects, particularly in road infrastructure and foundation layers. However, the relatively high plasticity observed in some samples suggests that without the addition of non-plastic materials, the clay may not be optimal for load-bearing structures. Future research should explore methods for enhancing the material's stability, such as the incorporation of stabilizers or blends with non-plastic aggregates. Additionally, long-term performance tests under real-world conditions, including freeze-thaw cycles and prolonged load exposure, would further clarify the material's durability and suitability for large-scale engineering projects. Ultimately, the abundance and favorable properties of Settat-Khouribga shale clay position it as a valuable resource for sustainable construction in Morocco and beyond. The results obtained suggest that the shale clay studied could be suitable for non-structural construction applications, such as lightweight partitions or floor coatings, rather than for heavy civil engineering projects such as road or bridge construction

References

[1] Abdelaziz M, Tammal M, Elbouhaddioui M, Gasmi EH. Apport des Données Géophysiques et géologiques à la mise en évidence de nouveaux éléments structuraux associés à la flexure de Settat (maroc central). Academia.edu. 2015.
[2] Mkrtchyan RV, Ismatov AA, Musaev RA. Clay shale from the dzherdanakskoe deposit: A high-quality ceramic material. Glass Ceram. 2002;177-9. https://doi.org/10.1023/A:1020428012963
[3] El Bouqdaoui K. Geological and Geotechnical Study of the City of Settat. Geotechnical Mapping and Useful Substances of the Settat Province. Third-Cycle Doctoral Thesis. 1995.
[4] NF P08-301. Vertical building elements. Impact resistance tests. Impact bodies. Prinicple and general test procedures. April 1991.
[5] AFNOR. NF P 94-100: Sols: Reconnaissance et essais. Matériaux traités à la chaux et/ou aux liants hydrauliques- Essais d'évaluation de l'aptitude d'un sol au traitement. 1999.
[6] Fetisov GV. X-ray diffraction methods for structural diagnostics of materials: Progress and achievements. 2020;2-32. https://doi.org/10.3367/UFNe.2018.10.038435

[7] Asef M, Farrokhrouz M. Shale engineering: mechanics and mechanisms. CRC Press; 2013. https://doi.org/10.1201/b13825
[8] Seedsman RW. Characterizing clay shales. In: Rock Testing and Site Characterization. Pergamon; 1993. p. 151-65. https://doi.org/10.1016/B978-0-08-042066-0.50014-8
[9] El Hassani A. Evolution des sciences géologiques à l'Institut Scientifique. 2020.
[10] Jeannette A, Gigout M. Minerais et substances utiles. Notice explicative. Carte géologique de la Meseta marocaine entre Settat et Mazagan (El Jadida)(Doukkala et Chaouïa occidentale). 1965;25-8.
[11] Elfirdoussi A, El Amrani Paaza N, Soulaimani A. Hydrogeological characterization of Settat Ben Ahmed Plateau Aquifer (central morocco). 2024. https://doi.org/10.1051/e3sconf/202448906002
[12] Pokorny AG. Classification des granulats pour les couches de Roulement des Chaussees. Bull Int Assoc Eng Geol. 1984;30(1):119-21. https://doi.org/10.1007/BF02594291
[13] El Hammouti A, Charai M, Mezrhab A, Nasri H, Karkri M. Effect of the nature of clayey soils (Eastern Morocco) on the thermophysical properties of bricks. Mater Today Proc. 2022;321-7. https://doi.org/10.1016/j.matpr.2022.01.233
[14] IMANOR. NM 13.1.008: Analyse granulométrique des sols par tamisage. 1998.
[15] NF EN 1097-2. Granulats - Los Angeles. 2010.
[16] IMANOR. NM 13.1.128: Sols: Reconnaissance et essais - Indice CBR après immersion - Indice CBR immédiat - Indice Portant Immédiat - Mesure sur échantillon compacté dans le moule CBR. 2019.
[17] IMANOR. NM 13.1.007: Essai d'identification: Détermination des limites d'ATTERBERG- Limite de plasticité au rouleau- Limite de liquidité à la coupelle. 1998.
[18] NF EN 14157. Résistance à l'abrasion / usure. 2020.
[19] ASTM D422-63(2007)e2. Standard Test Method for Particle-Size Analysis of Soils. n.d.
[20] ASTM C131/C131M-20. Standard Test Method for Resistance to Degradation of Small-Size Coarse Aggregate by Abrasion and Impact in the Los Angeles Machine. n.d.
[21] ASTM D4318-17e1. Standard Test Methods for Liquid Limit, Plastic Limit, and Plasticity Index of Soils. n.d.
[22] Mohammed A, Abdullah A. Scanning electron microscopy (SEM): A review. In: Proceedings of the 2018 International Conference on Hydraulics and Pneumatics-HERVEX, Băile Govora, Romania. 2018. p. 7-9.
[23] Hafidi A. Catalogue des structures types de Chaussées Neuves. Service d'études techniques des routes et Autoroutes Laboratoire Central des Ponts et Chaussées. 2019.
[24] ASTM D422-63. Standard Test Method for Particle-Size Analysis of Soils. 2007.
[25] ASTM D6928. Standard Test Method for Resistance of Coarse Aggregate to Degradation by Abrasion in the Micro-Deval Apparatus. 2017.
[26] ASTM C131/C131M-20. Standard Test Method for Resistance to Degradation of Small-Size Coarse Aggregate by Abrasion and Impact in the Los Angeles Machine. 2020.
[27] Li S, Zhao J, Guo H, Wang H, Li M, Li J, et al. A viscoplasticity model for shale creep behavior and its application on fracture closure and conductivity. Energies. 2024;1122. https://doi.org/10.3390/en17051122
[28] Putera AM, Pramusandi S, Damianto B. Identification and classification of clayshale characteristic and some considerations for slope stability. Afr J Environ Sci Technol. 2017;11(4):163-97. https://doi.org/10.5897/AJEST2014.1792

[29] Saberian M, Li J, Perera ST, Zhou A, Roychand R, Ren G. Large-scale direct shear testing of waste crushed rock reinforced with waste rubber as pavement base/subbase materials. Transp Geotech. 2021;28:100546. https://doi.org/10.1016/j.trgeo.2021.100546
[30] Bouzeboudja A, Melbouci B. Etude de l'evolution de la dimension fractale des grains de materiaux granulaires soumis a des Essais Mecaniques. 2015;821-39. https://doi.org/10.1007/s10064-015-0825-7
[31] Jones C, Mulloy B, Sanderson MR. Crystallographic methods and protocols. Humana Press. 1996. https://doi.org/10.1385/0896032590
[32] Ben Ouakkass M, Ouadif L, Akhssas A, Bahi L. Study of the degradation of the geometry of the railway between the PK 80 and 105 at the plateau of Settat (Morocco). MATEC Web Conf. 2018;149. https://doi.org/10.1051/matecconf/201814902021
[33] Lyu Q, Lyu Q, Hu C, Dick JM, Shi J, Tan J. Experimental study on the mechanical properties of shale after long-term immersion in fracturing fluids with different pH. 2022;5047-61. https://doi.org/10.1007/s00603-022-02918-4
[34] Melbouci B. Étude du phénomène d'écrasement des grains de schiste au compactage. Rev Fr Geotech. 2006;29-37. https://doi.org/10.1051/geotech/2006117029
[35] Boumehraz M, Boucetta F, Mellas A, Meghaichi NEH, Chebah M. Comportement mécanique du schiste traité par des ajouts du ciment et de la chaux. 2020.
[36] Hsu SC, Nelson PP. Characterization of cretaceous clay-shales in North America. Geot Eng Hard Soils-Soft Rocks. 1993.
[37] Abd Ellatief M, Mahmoud M, Abdo H. Geotechnical properties of expansive clay shale in El-MAHROWSA, Qena, Egypt. Eng Geol Geol Eng Sustain Use Earth's Resour Urbanization Infrastruct Prot Geohazards. 2017;41-62. https://doi.org/10.1007/978-3-319-61648-3_3
[38] Addad S, Melbouci B. Influence de la pollution des eaux sur la dégradation des roches schisteuses. 2019.
[39] Bonini M, Debernardi D, Barla M, Barla G. The mechanical behaviour of clay shales and implications on the design of tunnels. 2007. https://doi.org/10.1007/s00603-007-0147-6
[40] Goldstein JI, Newbury DE, Michael JR, et al. Scanning electron microscopy and X-ray microanalysis. Springer. 2017. https://doi.org/10.1007/978-1-4939-6676-9
[41] Tuffour YA, Banini SY, Adams CA. Investigation of Afram Shale for road construction. Am J Civ Eng Archit. 2016;4(3):80-3.
[42] Xiang-Rong Y, De-Tian Y, Xiao-Song W, et al. Different formation mechanism of quartz in siliceous and argillaceous shales: A case study of Longmaxi Formation in South China. Mar Pet Geol. 2018;94:80-4. https://doi.org/10.1016/j.marpetgeo.2018.03.036
[43] Erdogmus E, Sutcu M, Gencel O, Kazmi SMS, Munir MJ, Velasco PM, Ozbakkaloglu T. Enhancing thermal efficiency and durability of sintered clay bricks through incorporation of polymeric waste materials. J Clean Prod. 2023;420:138456. https://doi.org/10.1016/j.jclepro.2023.138456
[44] Johan A, Sugianto A, Rahardjo PP. Replacement of Weathered Clay Shale Using Soil Cement for Bridge Approach Embankment in Purwakarta-Indonesia. Indones Geotech J. 2023;2(3):123-38. https://doi.org/10.56144/igj.v2i3.58